Research Article | Vol. 8, No. 4 | 1 Apr 2017 | BIOMEDICAL OPTICS EXPRESS 2245
Biomedical Optics EXPRESS

Photoacoustic reflection artifact reduction using photoacoustic-guided focused ultrasound: comparison between plane-wave and element-by-element synthetic backpropagation approach

MITHUN KUNIYIL AJITH SINGH,[1,*] MICHAEL JAEGER,[2] MARTIN FRENZ,[2] AND WIENDELT STEENBERGEN[1]

[1]*Biomedical Photonic Imaging Group, MIRA institute for Biomedical Technology and Technical Medicine, University of Twente, P.O. Box 217, 7500 AE Enschede, The Netherlands*
[2]*Institute of Applied Physics, University of Bern, Sidlerstrasse 5, 3012 Bern, Switzerland*
**m.kuniyilajithsingh@utwente.nl*

Abstract: Reflection artifacts caused by acoustic inhomogeneities constitute a major problem in epi-mode biomedical photoacoustic imaging. Photoacoustic transients from the skin and superficial optical absorbers traverse into the tissue and reflect off echogenic structures to generate reflection artifacts. These artifacts cause difficulties in the interpretation of images and reduce contrast and imaging depth. We recently developed a method called PAFUSion (photoacoustic-guided focused ultrasound) to circumvent the problem of reflection artifacts in photoacoustic imaging. We already demonstrated that the photoacoustic signals can be backpropagated using synthetic aperture pulse-echo data for identifying and reducing reflection artifacts *in vivo*. In this work, we propose an alternative variant of PAFUSion in which synthetic backpropagation of photoacoustic signals is based on multi-angled plane-wave ultrasound measurements. We implemented plane-wave and synthetic aperture PAFUSion in a handheld ultrasound/photoacoustic imaging system and demonstrate reduction of reflection artifacts in phantoms and *in vivo* measurements on a human finger using both approaches. Our results suggest that, while both approaches are equivalent in terms of artifact reduction efficiency, plane-wave PAFUSion requires less pulse echo acquisitions when the skin absorption is the main cause of reflection artifacts.

OCIS codes: (170.5120) Photoacoustic imaging; (170.7170) Ultrasound; (170.3880) Medical and biological imaging.

References and links

1. Y. Zhou, J. Yao, and L. V. Wang, "Tutorial on photoacoustic tomography," J. Biomed. Opt. **21**(6), 061007 (2016).
2. P. Beard, "Biomedical photoacoustic imaging," Interface Focus **1**(4), 602–631 (2011).
3. V. Ntziachristos, "Going deeper than microscopy: the optical imaging frontier in biology," Nat. Methods **7**(8), 603–614 (2010).
4. M. Heijblom, D. Piras, F. M. van den Engh, M. van der Schaaf, J. M. Klaase, W. Steenbergen, and S. Manohar, "The state of the art in breast imaging using the Twente Photoacoustic Mammoscope: results from 31 measurements on malignancies," Eur. Radiol. **26**(11), 3874–3887 (2016).
5. S. A. Ermilov, T. Khamapirad, A. Conjusteau, M. H. Leonard, R. Lacewell, K. Mehta, T. Miller, and A. A. Oraevsky, "Laser optoacoustic imaging system for detection of breast cancer," J. Biomed. Opt. **14**(2), 024007 (2009).
6. P. van Es, S. K. Biswas, H. J. Bernelot Moens, W. Steenbergen, and S. Manohar, "Initial results of finger imaging using photoacoustic computed tomography," J. Biomed. Opt. **19**(6), 060501 (2014).
7. X. L. Dean-Ben and D. Razansky, "Adding fifth dimension to optoacoustic imaging: volumetric time-resolved spectrally enriched tomography," Nat. Light Sci. Appl. **3**(1), 137 (2014).
8. A. Hussain, W. Petersen, J. Staley, E. Hondebrink, and W. Steenbergen, "Quantitative blood oxygen saturation imaging using combined photoacoustics and acousto-optics," Opt. Lett. **41**(8), 1720–1723 (2016).

#283578 https://doi.org/10.1364/BOE.8.002245
Journal © 2017 Received 3 Mar 2017; revised 6 Mar 2017; accepted 13 Mar 2017; published 20 Mar 2017

Biomedical Optics EXPRESS

9. M. Kuniyil Ajith Singh, W. Steenbergen, and S. Manohar, "Handheld Probe-Based Dual Mode Ultrasound/Photoacoustics for Biomedical Imaging," in *Frontiers in Biophotonics for Translational Medicine* (Springer, 2016), pp. 209–247.
10. M. Jaeger, J. C. Bamber, and M. Frenz, "Clutter elimination for deep clinical optoacoustic imaging using localised vibration tagging (LOVIT)," Photoacoustics **1**(2), 19–29 (2013).
11. M. Jaeger, D. Harris-Birtill, A. Gertsch, E. O'Flynn, and J. Bamber, "Deformation-compensated averaging for clutter reduction in epiphotoacoustic imaging in vivo," J. Biomed. Opt. **17**(6), 066007 (2012).
12. M. Kuniyil Ajith Singh and W. Steenbergen, "Photoacoustic-guided focused ultrasound (PAFUSion) for identifying reflection artifacts in photoacoustic imaging," Photoacoustics **3**(4), 123–131 (2015).
13. M. Kuniyil Ajith Singh, M. Jaeger, M. Frenz, and W. Steenbergen, "In vivo demonstration of reflection artifact reduction in photoacoustic imaging using synthetic aperture photoacoustic-guided focused ultrasound (PAFUSion)," Biomed. Opt. Express **7**(8), 2955–2972 (2016).
14. H. M. Schwab, M. F. Beckmann, and G. Schmitz, "Photoacoustic clutter reduction by inversion of a linear scatter model using plane wave ultrasound measurements," Biomed. Opt. Express **7**(4), 1468–1478 (2016).
15. E. J. Alles, M. Jaeger, and J. C. Bamber, "Photoacoustic Clutter Reduction Using Short-Lag Spatial Coherence Weighted Imaging," In proceedings of IEEE International Ultrasonics Symposium (IUS, 2014), pp. 41–44.
16. X. L. Deán-Ben, V. Ntziachristos, and D. Razansky, "Artefact reduction in optoacoustic tomographic imaging by estimating the distribution of acoustic scatterers," J. Biomed. Opt. **17**(11), 110504 (2012).
17. K. Wapenaar, J. Thorbecke, and J. van der Neut, "A single-sided homogeneous Green's function representation for holographic imaging, inverse scattering, time-reversal acoustics and interferometric Green's function retrieval," Geophys. J. Int. **205**(1), 531–535 (2016).
18. K. Daoudi, P. J. van den Berg, O. Rabot, A. Kohl, S. Tisserand, P. Brands, and W. Steenbergen, "Handheld probe integrating laser diode and ultrasound transducer array for ultrasound/photoacoustic dual modality imaging," Opt. Express **22**(21), 26365–26374 (2014).
19. M. Jaeger, S. Schüpbach, A. Gertsch, M. Kitz, and M. Frenz, "Fourier reconstruction in optoacoustic imaging using truncated regularized inverse k-space interpolation," Inverse Probl. **23**(6), S51–S63 (2007).
20. M. A. Lediju Bell, N. P. Kuo, D. Y. Song, J. U. Kang, and E. M. Boctor, "In vivo visualization of prostate brachytherapy seeds with photoacoustic imaging," J. Biomed. Opt. **19**(12), 126011 (2014).
21. W. Xia, D. I. Nikitichev, J. M. Mari, S. J. West, R. Pratt, A. L. David, S. Ourselin, P. C. Beard, and A. E. Desjardins, "Performance characteristics of an interventional multispectral photoacoustic imaging system for guiding minimally invasive procedures," J. Biomed. Opt. **20**(8), 086005 (2015).
22. M. Kuniyil Ajith Singh, V. Parameshwarappa, E. Hendriksen, W. Steenbergen, and S. Manohar, "Photoacoustic-guided focused ultrasound for accurate visualization of brachytherapy seeds with the photoacoustic needle," J. Biomed. Opt. **21**(12), 120501 (2016).
23. G. Held, S. Preisser, H. G. Akarçay, S. Peeters, M. Frenz, and M. Jaeger, "Effect of irradiation distance on image contrast in epi-optoacoustic imaging of human volunteers," Biomed. Opt. Express **5**(11), 3765–3780 (2014).
24. S. Preisser, G. Held, H. G. Akarçay, M. Jaeger, and M. Frenz, "Study of clutter origin in in-vivo epi-optoacoustic imaging of human forearms," J. Opt. **18**(9), 094003 (2016).

1. Introduction

Photoacoustic (PA) imaging (optoacoustic imaging) allows the detection of optical absorption contrast inside optically scattering tissue via ultrasound (US) detection of thermoelastically induced US, when irradiating the tissue with pulsed laser light [1, 2]. This technique offers great promise in a wide range of pre-clinical and clinical applications [3–7].

Since PA imaging involves detection of US signals, integration with conventional pulse-echo US in a single multi-modal device is a logical development. A PA image superimposed on a US image can give anatomical and structural information overlaid with complementary functional information of e.g. the local blood oxygenation level in a multi-wavelength approach [8]. Handheld dual mode US/PA probes use an epi-illumination geometry, where the optical components are integrated with the US probe to irradiate the tissue from the same side where PA signals are detected [9]. Epi-PA imaging provides freehand probe guidance and large flexibility in imaging different body parts [10]. On the downside, high light fluence beneath the US probe results in strong PA signals from the skin and superficial blood vessels. These PA transients will traverse into the tissue and reflect off the echogenic structures to generate reflection artifacts (echo clutter) [10–16], that can significantly reduce contrast and imaging depth [10, 13]. In addition, reflection artifacts just beneath the skin and in close proximity to blood vessels may confuse diagnosis by being misinterpreted as additional blood vessels or by biasing multi-wavelength imaging results. Thus, it is important to identify and reduce in-plane reflection artifacts for clinically successful high-contrast deep tissue epi-PA imaging.

Biomedical Optics EXPRESS

Several approaches for identifying and reducing reflection artifacts have been reported [10–12, 14–16]. We recently reported on our first *in vivo* results of photoacoustic-guided focused ultrasound (PAFUSion) [13]. PAFUSion is based on the assumptions that significant artifacts stem only from PA transients that are generated by superficial absorbers (i.e. melanin or superficial blood vessels) and are reflected by deeper structures, and that the resulting echoes are temporally separated from the direct PA signal of these transients. Then it is possible to mimic reflection artifacts via backpropagation without introducing new artifacts. The PA signals were virtually backpropagated using synthetic aperture US data for imitating the inward-travelling PA field and thus the resulting reflection artifacts. Subtraction of the imitated reflection artifacts from the original PA data resulted in an artifact-reduced image. Synthetic aperture US data were defined as the echoes collected after transmission of US from each element, one at a time.

To enable artifact reduction also when the direct signal and the echoes from strong PA transients overlap in time, alternative approaches have been proposed. Schwab *et al.* [14] developed an inverse scattering model based on the Born approximation. Starting from a single-sided Green's function representation for time-reversal acoustics [17], Van der Neut *et al.* developed a single-sided representation for backpropagation of PA signals based on the multidimensional Marchenko equation. Whereas PAFUSion and the inverse scattering approach are limited to echoes that occur at tissue below the optical absorbers, the Marchenko equation approach is also able to correct for reflections that occur at superficial tissue structures both below and above strong PA sources. Such reflections may be significant when reverberating in-between tissue layers. Whereas these promising approaches are still under development, PAFUSion is experimentally less demanding and was already successfully demonstrated *in vivo*.

In this study, we focus on PAFUSion and propose a modification of this technique where synthetic backpropagation is based on multi-angled plane-wave transmissions as opposed to element-by-element transmission of US. The goal of this study was a quantitative comparison of reflection artifact reduction achieved using plane-wave and synthetic aperture PAFUSion implemented in a handheld US/PA imaging system. We demonstrate strong in-plane artifact reduction using both methods in a phantom as well as *in vivo* measurements on a finger of a human volunteer. Both approaches are systematically compared to conclude on the most suitable implementation in a clinical scenario.

2. Theory

In general, PAFUSion mimics the PA wavefield traversing into the tissue and thus the resulting reflection artifacts by using US transmissions [12, 13]. In the optimum case, this shall allow to subtract the identified artifacts from the PA signal and thus obtain a reflection-artifact-free PA image. In the less optimal case where full subtraction is not possible, this allows the identification of reflection artifacts as such, and thus a more accurate interpretation of "true" PA features.

PAFUSion using backpropagation [13] is based on the concept that the PA wave field can be decomposed into an outward-travelling part (P_O) that is detected as "true" PA signal by the transducer, and an inward-travelling part (P_i) that reflects off the echogenic structures to generate reflection artifacts (Fig. 1(a)). At time $t = 0$, the two wave fields are identical but move in opposite directions. Thus, backpropagation of the wave field that was detected within the time interval $[0, T]$ reproduces after time T the inward travelling wave field (Fig. 1(b)). The choice of T is illustrated in Fig. 1(a): It encompasses the direct signal of superficial absorbers (e.g. skin) but excludes the part of the signal where echoes become significant. The US echoes obtained after backpropagation will be similar to the reflection artifacts in the PA image. Physical backpropagation of PA signals requires the capability of transmitting arbitrarily shaped signals, which is beyond state-of-the-art of US equipment. In our previous work, we demonstrated the potential of using element-by-element US data (like in synthetic

Biomedical Optics EXPRESS

aperture (SA) imaging) to synthetically backpropagate PA signals and thus identify and reduce reflection artifacts [13]. Synthetic aperture PAFUSion involves convolution of the time-inverted PA signal from each element with the tissue impulse response (defined as the echoes detected after transmission of a Dirac delta US pulse on the respective element), and subsequent superposition of the results for all elements. The resulting synthetized data mimic the PA reflection artifacts and are used to correct the PA images to obtain reflection-artifact-free PA images. Figure 1(c) illustrates the synthetic backpropagation of skin PA signal using synthetic aperture transmission of US. In this case, it is obvious that a scan through the whole aperture, with one element transmitting at a time, is required to mimic the inward travelling PA wave field even in the simple case where the skin layer is the only prominent artifact-generating PA source.

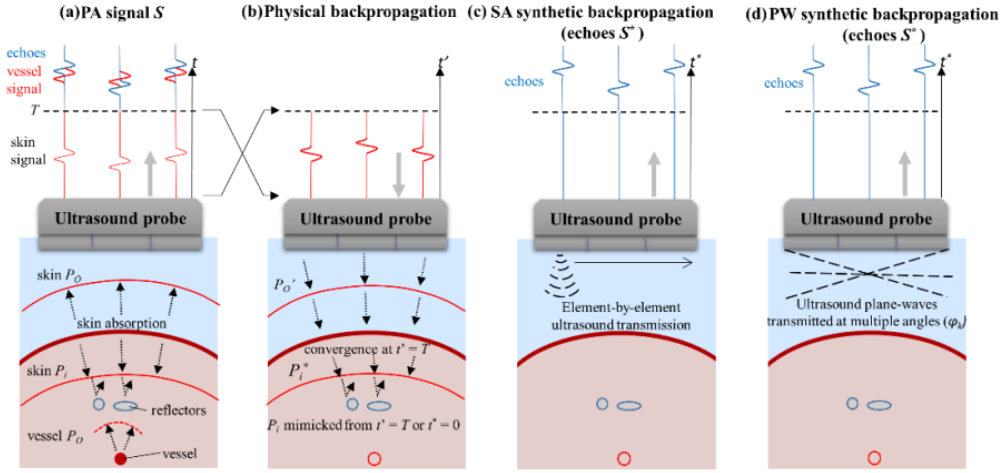

Fig. 1. (a) Illustration of inward (P_i propagating into the tissue) and outward-propagating (P_O propagating towards the probe) PA transients, generated by optical absorption in the skin melanin layer. (b) Time-inversion and backpropagation of the PA signal from interval $t = [0, T]$ towards mimicking the PA wavefield P_i* traversing into the tissue and identification of resulting echoes. Alternative to physical backpropagation, synthetic backpropagation can be based on reference pulse-echo data that is acquired with (c) element-by-element US transmissions (like in synthetic aperture imaging), or (d) transmission of plane-waves (PA) with multiple angles.

While the synthetic aperture approach is conceptually simple, other ways of generating reference pulse-echo data are possible and may be more efficient depending on the spatial distribution of artifact-generating PA sources. In the case where skin absorption is the main cause of reflection artifacts, the strong PA transient generated by the skin is close to a plane transient, and therefore a superposition of a sparse number of plane transients may be sufficient to mimic most part of the PA wavefield. This hypothesis inspired the implementation of an alternative approach, where virtual backpropagation is based on US plane-wave acquisitions with different transmit steering angles instead of the element-by-element US transmissions (Fig. 1(d)). In analogy to the description of synthetic backpropagation algorithm in our previous paper [13], step by step explanation of plane-wave PAFUSion is as follows:

1. Probe the tissue impulse response $S_{\delta k}(n^*,t'')$ by acquiring reference plane wave pulse-echo data detected on elements n^* after transmission with transmission angles φ_k
2. Decompose the PA signals $S(n,t)$ into components $\hat{S}(\varphi_k, t)$ that are generated by the part of the photoacoustic wavefield propagating into directions φ_k. The decomposition is implemented by directional filtering, using a delay-and-sum

Biomedical Optics EXPRESS

beamforming approach: Time-delay $S(n,t)$ for each element by delay $\tau(\varphi_k, n)$ that corresponds to the arrival time of a plane wave under angle φ_k at elements n. Average over n, resulting in signal $\hat{S}(\varphi_k, t)$:

$$\hat{S}(\phi_k, t) = \frac{1}{N}\sum_{n=1}^{N} S\left(n, t+\tau(n)\right), \quad \tau(n) = -\frac{\sin\phi_k \cdot x_n}{c} \tag{1}$$

3. Convolve $\hat{S}(\varphi_k, T\text{-}t')$ with $S_{\delta k}(n^*, t'')$ to obtain Signals $S^*(n^*, \varphi_k, t'')$
4. Superpose $S^*(n^*, \varphi_k, t'')$ by summing over angles φ_k and shift in time according to $t^* = t'' - T$ to obtain $S^*(n^*, t^*)$

S^* simulates the reflection artifacts in the PA signal.

3. Materials and methods

3.1 Equipment and setup

For all the experiments in this study, a handheld probe-based dual mode PA/US system was used [18]. Figure 2 shows the illustration of the system in which a commercial US scanner (MyLabOne, Esaote Europe BV, The Netherlands) is used along with a probe that integrates an US array with a diode laser module. The module produced pulses at 805 nm wavelength, 130 ns pulse width at an energy of 1 mJ per pulse, with a high pulse repetition frequency of up to 10 kHz. The US probe has a −6 dB fractional bandwidth of around 100% and center frequency of 7.5 MHz. For avoiding optical absorption in the acoustic lens surface, the aperture was optically shielded with a 10 µm thin gold foil.

The US scanner was used in research mode that provides access to all transmission and acquisition parameters. Custom-made software running on a laptop (connected to the scanner using USB 2.0 connection) controls the US scanner's scan sequence for triggering laser diodes, US transmission and the sequential switching between PA, synthetic aperture US, and multi-angled plane-wave US measurements (including important parameters such as the number of elements to transmit for synthetic aperture US and the number of angles for plane-wave US measurements). The system can read data from 64 channels at a time with a sampling rate of 50 MHz, and perform continuous data transfer for real-time processing running on the laptop. For both the phantom and *in vivo* studies, 64 middle elements of the aperture were used for synthetic aperture US (one element transmits at a time resulting in 64 acquisitions) and angles of −16° to + 16° with a step of 1° for plane-wave US measurements (resulting in 33 acquisitions). 200 frames of PA data were also saved for further processing. PA, plane-wave and synthetic aperture US measurements were performed with a repetition rate of 200 Hz resulting in an acquisition time of less than 2 seconds (acquisition of PA, synthetic aperture US and plane-wave US data). All the post-processing presented was performed offline, including image reconstruction using a frequency domain algorithm [19].

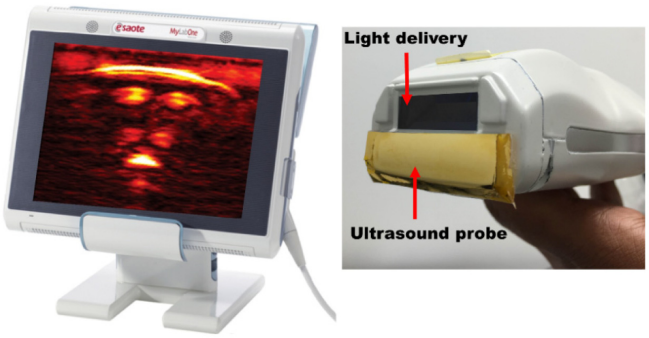

Fig. 2. Illustration of the commercial US system showing a real-time reconstructed PA image of a human finger (left) and the hybrid probe (right) integrating the laser module and the US transducer array (US probe is optically shielded with gold foil).

Biomedical Optics EXPRESS

3.2 Plane-wave and synthetic aperture PAFUSion – data processing

The processing steps for synthetic aperture PAFUSion are the same as described in our previous work [13]. Plane-wave PAFUSion was performed following the steps described in the Theory section. Echoes obtained by transmission of multi-angled plane-waves were used as the reference for synthetic backpropagation. PA signals were filtered for different directions corresponding to the angles used for US transmission and convolved with the pulse-echo data for that particular angle transmission. Superposition of convolution results for all the angles generates S*, which simulates reflection artifacts in the PA signal. S^* was subtracted from the PA signal (S) to generate the corrected PA signal without reflection artifacts.

In the backpropagation approach, Dirac delta transmit and receive impulse responses are implicitly assumed. However, the transducer elements typically show a resonant behaviour. As a result, the synthetically generated reflection signal S^* is a convolution of the real reflection signal S with the combined transmit and receive impulse response h, resulting in different temporal profiles of S and S^*. To compensate for the influence of h and thus enable accurate subtraction, the waveforms of S and S^* were convolved with a pair of finite impulse response (FIR) filters F and F^*, respectively. F applied a band-pass to S, to reduce low SNR spectral content outside the resonance of the transducer. F^* was applied to S^*. By solving a linear inverse problem, the filter coefficients were determined so that the convolution of F^* with h was identical to F. In other words, F^* performed a regularized deconvolution of S^*, and F matched S to the deconvolution result. The transducer response was determined in a pulse-echo experiment using a plane steel reflector.

Even after matching the waveforms, the PA image and the PAFUSion image (before envelope detection) typically show differences in amplitude and phase that are spatially dependent and lead to subtraction errors if not accounted for (see experimental results). To account for these differences and enable efficient correction of reflection artifacts, the amplitudes and phases of the identified artifacts in the PAFUSion image were matched to the respective counterpart in the PA image before subtraction. This was done by manually choosing a square region of interest (ROI) around a respective artifact. Within that ROI, the per-pixel Hermitian product between the complex-valued amplitudes (after Hilbert transform) in the PA image and the PAFUSion image was calculated, averaged over the ROI, and divided by the mean-square absolute amplitude of the PAFUSion image inside the ROI. This resulted in a single complex number, where the absolute value was the ratio between the mean-square feature amplitude of the PA image and the PAFUSion image, and the phase angle was the phase shift. Multiplication of the complex-valued PAFUSion image with that number thus resulted in matching of the amplitude and phase to the PA image inside the chosen ROI.

For the phantom measurement, the amplitude and phase matching was performed for every identified artifact separately to generate multiple corrected PA images (each with one artifact eliminated). For the *in vivo* measurement where many PA features and artifacts were present, amplitude and phase matching was performed for only one of the identified artifacts (one step subtraction by matching the amplitude and phase of one identified artifact with its counterpart in the PA image) for ease of interpretation and to avoid numerous corrected PA images.

3.3 Phantom experiment

Figure 3(a) shows the schematic of the phantom and the orientation of the US/PA probe used for the comparison of plane-wave and synthetic aperture PAFUSion. The phantom consisted of two optical absorbers (brown nylon threads, 0.28 mm diameter) positioned above and below an acoustic reflector (Delrin rod, 1.9 mm diameter). The optical absorbers as well as the acoustic reflector were embedded inside gelatin, in such a way that they were perpendicular to the imaging plane of the US transducer. A thin layer of black ink mixed with

Biomedical Optics EXPRESS

gelatin (India ink,~ 200 µm) was added to the surface of the gelatin phantom to mimic the optical absorption by the skin melanin layer and thus generating reflection artifacts. A water layer in-between the phantom surface and the US probe was used for acoustic coupling. This phantom was used to study reflection artifacts caused by both the extended PA features (eg: skin) and vessel-like features, and to compare the performance of plane-wave and synthetic aperture PAFUSion with these features. No optical scattering agent was added to the bulk of the gelatin phantom, to maximize the amplitude of the PA transients (and thereby of the PA reflections). In this experiment, the time *T* was chosen to be 8 µs, so as to backpropagate the PA signals from the skin-mimicking surface and the first nylon thread.

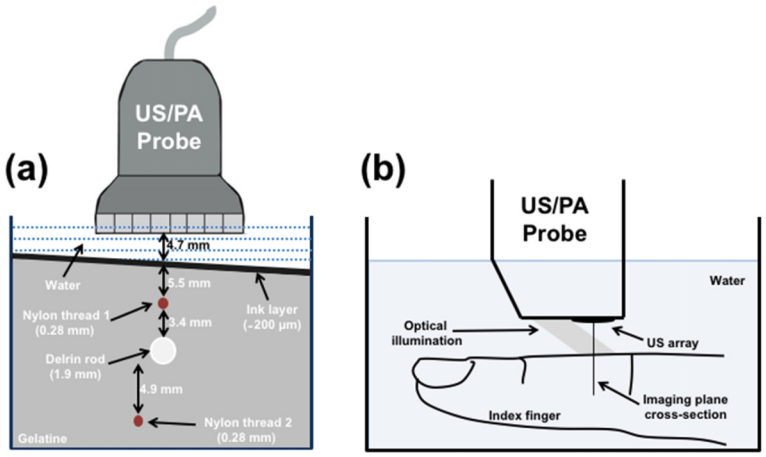

Fig. 3. (a) Schematic of the phantom and orientation of the US/PA probe, (b) Illustration of the *in vivo* measurement setup in which the imaging plane, cross-section of imaging plane with finger, water spacing between finger and probe, and the path of the optical beam are shown.

3.4 In vivo experiment – human finger

An evaluation of plane-wave and synthetic aperture PAFUSion for the reduction of reflection artifacts *in vivo* was performed in measurements on the index finger of a human volunteer with dusky skin complexion. The finger was positioned inside a water bath in such a way that the imaging plane was aligned perpendicular to the finger (between the distal interphalangeal joint and proximal interphalangeal joint in the sagittal part) as shown in Fig. 3(b). Real-time PA reconstruction provided a feedback to select the location for the measurements. For *in vivo* measurements, *T* was selected in such a way that the PA signals from only the skin and the superficial blood vessels were synthetically backpropagated for performing PAFUSion.

3.5 Quantitative comparison of plane-wave and synthetic aperture PAFUSion

Performance of plane-wave and synthetic aperture PAFUSion is compared based on the efficiency in reducing reflection artifacts. For this purpose, pixel intensities of selected regions of interest (ROI) in the image are compared, before and after correction of PA images using plane-wave and synthetic aperture PAFUSion. The pixel intensity of a ROI was calculated as the average intensity of 9 pixels (3 by 3) centered around the maximum intensity value in the area. All features with pixel intensities higher than 1 dB were used for comparison and some of them are discussed in detail in the results section. Pixel intensities of the same selected regions were determined in the uncorrected (PA_i) and in the corrected PA image ($CorrPA_i$). The ratio of PA_i and $CorrPA_i$ (Intensity reduction ratio = $PA_i/CorrPA_i$) was calculated and expressed in dB. In the phantom experiment where correction was optimized for different features separately, the CorrPAi value for each feature was determined in the respective corrected PA image. The intensity reduction ratio obtained for different ROIs using

Biomedical Optics EXPRESS

plane-wave and synthetic aperture PAFUSion are compared to conclude on the performance of both the approaches in reflection artifact reduction.

4. Results

In all images, lateral and axial coordinates are represented by x and z respectively. The squared envelope of the images (PA, US, PAFUSion and corrected PA) is shown in dB scale.

4.1 Phantom experiment

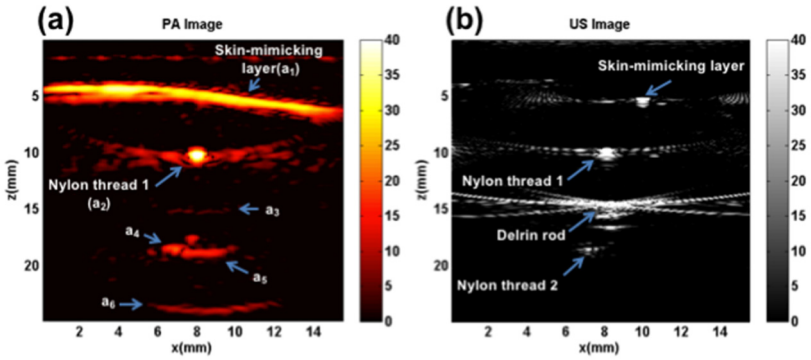

Fig. 4. Phantom experiment results: (a) PA image with several features marked (a_1 – a_6), (b) US image.

Figure 3 schematically illustrates the details of the phantom and the orientation of the hybrid PA/US probe in the experimental setup. Echoes from the skin-mimicking layer, nylon thread 1, nylon thread 2, and the Delrin rod are visible in the US image (Fig. 4(b)). The skin-mimicking layer is seen as a point-like feature most likely because of the inclined angle of the top surface of the phantom. Figure 4(a) shows the PA image of the phantom where multiple bright features are visible. The skin-mimicking layer (marked as a_1) and nylon thread 1 (marked as a_2) are visible in the PA image. Near the expected position of thread 2, there is a horizontally extended feature (a_5) visible which does not correspond to any optical absorbers in the phantom. This feature obscures the visibility of nylon thread 2, which would turn up as point-like structure at the location marked with a_4. In addition, there are two further features (a_3 and a_6) visible in the PA image.

Figure 5 shows the results of using plane-wave PAFUSion for identifying and reducing reflection artifacts in the phantom experiment. Figure 5(a) shows the PAFUSion image with all the identified reflection artifacts. Three of the features (a_3, a_5 and a_6) visible in the PA image (Fig. 4(a)) are identified as artifacts using plane-wave PAFUSion. Feature a_3 is weakly visible in the PAFUSion image (Fig. 5(a)) because of the chosen dB scale. Features a_3 and a_6 would have been caused by the reflection of the strong PA transient from the skin-mimicking layer on nylon thread 1 and Delrin rod respectively. Reflection of the nylon thread 1 signal on the Delrin rod would have resulted in the feature a_5. A reflection artifact was identified at the location of nylon thread 1 also. This may be the result of reflection of PA transient from nylon thread 1 reflecting off its own surface during signal generation. Alternatively and more probable this may be an artifact of the technique, caused by the reflection of the backpropagated wavefield at the absorber surface, immediately before it converges at $t^* = 0$. Irrespective of the source of this artifact, its pixel intensity is significantly lower than the actual PA signal from the nylon thread and does not affect any of the image correction steps as already discussed in [13]. Based on the very small relative amplitude compared to the other artifacts, this artifact was identified as false artifact based on visual inspection, and no artifact correction was performed in this region.

Biomedical Optics EXPRESS

Whereas the shape and spatial details of the identified reflection artifacts match the reflection artifacts in the PA image well, the relative amplitudes and phases of the identified artifacts were different from the artifacts in the PA image. Potential reasons for this behavior are: (i) The pulse-echo amplitude changes with depth owing to elevation focus, whereas – in backpropagation – we assume 2D sound propagation and therefore that there is no elevation focus. (ii) The spatial orientation of the PA sources which were maybe not perpendicular to the imaging plane, again violating the assumption of 2D sound propagation parallel to the imaging plane. For that reason, amplitude and phase of the identified artifacts had to be matched before subtracting from the PA image. In spite of the spatially dependent variations in phases and amplitudes, relative amplitudes of the actual identified artifacts were close to one. Figure 5(b)-5(d) shows the resulting corrected PA images (when amplitude and phase matching was performed for different artifacts) demonstrating optimum artifact reduction at the respective locations. In Fig. 5(b), the matching was achieved at the location of a_3. As a result, the pixel intensity of the feature a_3 is considerably reduced in the first corrected PA image (Fig. 5(b)) compared to the uncorrected one (Fig. 4(a)). Along with a_3, intensity of a_6 is also reduced. It is worth mentioning that the pixel intensities of the features which are not identified as artifacts (actual PA features) are not visibly changed. Figure 5(c) shows the corrected PA image in which pixel intensity of the feature a_5 is significantly reduced. In this case, amplitude and phase matching was performed separately for feature a_5. It is interesting to notice that the nylon thread 2 which was obscured by an artifact in the PA image becomes evident as a dot-like feature after the correction. This demonstrates the effectiveness of PAFUSion in revealing PA features that were initially obscured by reflection artifacts. In this case, even though the intensity of feature a_5 could be reduced, the intensity level of feature a_6 was increased. Figure 5(d) shows the last corrected PA image in which the amplitude and phase matching filters where adapted to reduce the intensity of feature a_6. Along with a_6, intensity of feature a_3 is also reduced. Different steps of amplitude and phase matching were thus required for reducing intensities of different artifacts, and partially some artifacts were increased while reducing others. The reason for this is the different relative amplitude and phase of different artifacts in the PAFUSion image as compared to the real PA image.

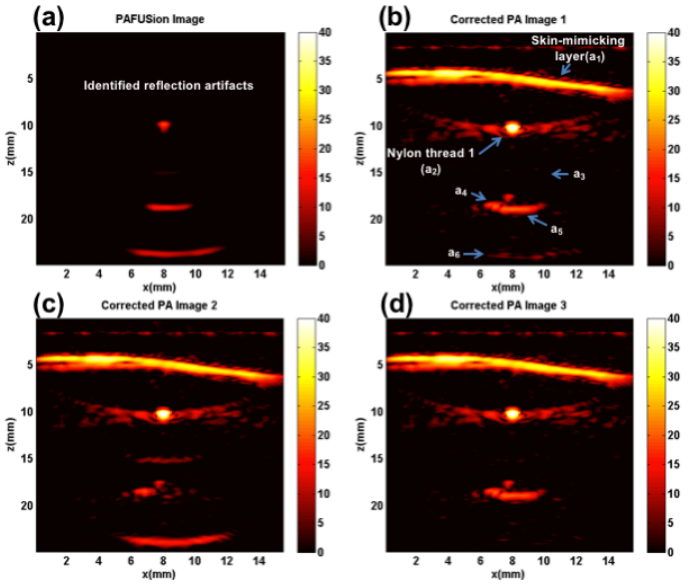

Fig. 5. Plane-wave PAFUSion to identify and reduce reflection artifacts in the phantom experiment: (a) PAFUSion image, and corrected PA images where the PAFUSion image was subtracted after matching amplitude and phase at the locations of the features a_3 (b), a_5 (c) and a_6 (d).

Biomedical Optics EXPRESS

The ratio of PA pixel intensities before and after correction was calculated for all the regions marked in the PA image (Fig. 4(a)). For the corrected PA pixel intensities at the location of different features, the corresponding corrected PA images were considered. For example, the corrected image value of feature a_6 was calculated from Fig. 5(d), where this feature was corrected. All the reflection artifact reduction ratio values are summarized in dB scale in Table 1 to quantitatively validate the efficiency of plane-wave PAFUSion in reducing reflection artifacts.

Figure 6 shows the results of using synthetic aperture PAFUSion for identifying and reducing reflection artifacts in the phantom experiment. As for the plane-wave PAFUSion results, all the artifacts are accurately identified and reduced using synthetic aperture PAFUSion. Both the approaches were equally capable of uncovering reflection artifacts caused by both an extended PA source (skin-mimicking layer) and a point-like PA source (nylon thread perpendicular to the probe). It is important to mention that plane-wave PAFUSion was performed with almost half number of acquisitions (33 acquisitions, double the frame rate) compared to the synthetic aperture approach (based on the hypothesis that a smaller number of plane transients can mimic the PA wavefield from skin). Reflection artifact reduction ratio values for all the marked features in the PA image are summarized in dB scale in Table 1 to quantitatively validate and compare the efficiency of synthetic aperture PAFUSion with plane-wave PAFUSion in reducing reflection artifacts. It is clear that both approaches are similar in terms of reflection artifact reduction efficiency. Using both the approaches, the amplitudes of identified reflection artifacts (a_3, a_5, and a_6) were reduced on an average of 14 dB substantiating that these are artifacts. On the other hand, pixel intensities of real PA features (a_1, a_2, and a_4) are not affected.

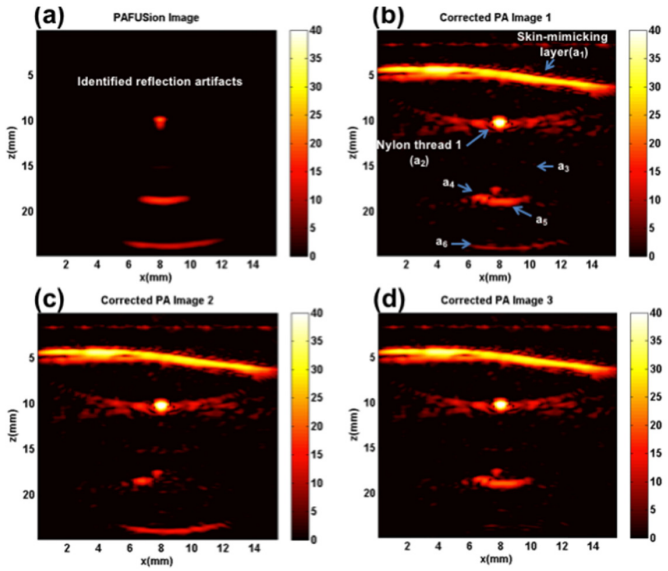

Fig. 6. Synthetic aperture PAFUSion to identify and reduce reflection artifacts in the phantom experiment: (a) PAFUSion image, and corrected PA images where the PAFUSion image was subtracted after matching amplitude and phase at the location of the feature a_3 (b), a_5 (c) and a_6 (d).

Biomedical Optics EXPRESS

Table 1. Comparison of Intensity Reduction Ratios (IRR) achieved using plane-wave and synthetic aperture PAFUSion for the phantom measurement

Region of interest	a_1	a_2	a_3	a_4	a_5	a_6
IRR (dB) (Plane-wave)	1	1.1	15	1	12	14.2
IRR (dB) (Synthetic aperture)	1	1.15	15.2	1	13.5	13.1

4.2 In vivo experiment

In vivo evaluation and comparison of plane-wave and synthetic aperture PAFUSion was performed on the index finger of a human volunteer. Figure 7(a) shows the PA image of the finger in which several bright features are visible. Some of the features are marked in the PA image for reference in Fig. 7(c). The high PA response from the skin melanin layer is visible as a bright arc-like feature (marked as a_1) at a depth of around z = 7 mm. Four bright features (a_2, a_3, a_4, and a_5) are visible just underneath the skin layer which might be superficial blood vessels. Apart from these, several diffuse features are visible beneath the skin and deeper inside the tissue, out of which some are marked (a_6, a_7, a_8, and a_9). Figure 7(b) shows the US image of the same location. Skin (z = 7mm), bone (z = 10 mm) and several other echogenic structures are visible in the US image.

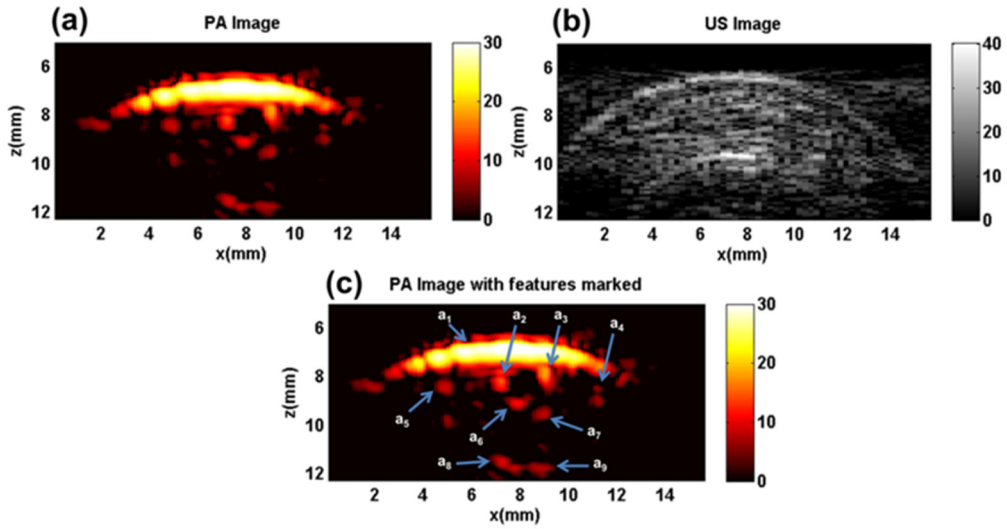

Fig. 7. *In vivo* experiment results: (a) PA image, (b) US image, (c) PA image with several features marked (a_1 – a_9).

Figure 8 shows the results of using plane-wave PAFUSion for identifying and reducing reflection artifacts in the *in vivo* experiment. The PAFUSion image (Fig. 8(a)) shows the reflection artifacts and demonstrates that the majority of the features in the PA image correlate with the simulated reflections. Except for a_1 – a_4, all other features in the PA image are exposed as reflection artifacts by using plane-wave PAFUSion. As in the phantom experiment, artifacts are identified at the depth of the skin melanin layer (z = 7 mm) whose relative pixel intensities are though far smaller than the actual PA signal from the skin. As hypothesized in a previous study and in the phantom experiment, this is most likely an artifact of the backpropagation approach. Many of the identified artifacts are in close proximity to

Biomedical Optics EXPRESS

superficial blood vessels. In an uncorrected image, features like a_5 – a_7 could therefore be easily misinterpreted as blood vessels, inflammation or a cancerous tissue.

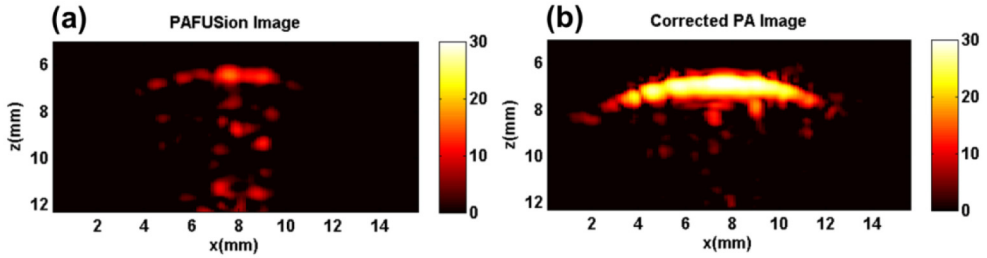

Fig. 8. Plane-wave PAFUSion to identify and reduce reflection artifacts in the *in vivo* measurement: (a) PAFUSion image, (b) corrected PA image.

Similar to the phantom experiment, the relative amplitudes and phases of the identified and the actual reflection artifacts are not identical for all artifacts, thus simultaneous correction of all artifacts with a single amplitude and phase matching step was not possible. For avoiding multiple images and discussion of results, correction of PA image is demonstrated by one-step amplitude and phase matching, which was adapted for reduction of one of the identified reflection artifacts (a_7). Another reason for a one-step correction strategy was, that the optimum correction step for a_7 simultaneously also reduced other artifacts to a certain extent. Figure 8(b) shows the corrected PA image in which the pixel intensities of identified artifacts are significantly reduced. Features a_6-a_9 almost completely disappeared in the corrected PA image. The intensity of the feature a_5 that may be interpreted as a blood vessel also is significantly reduced compared to the PA image. The ratios of PA pixel intensities before and after correction for all the regions marked in the PA image are summarized in Table 2 to quantitatively validate the efficiency of plane-wave PAFUSion in reducing reflection artifacts.

Figure 9 shows the results of PA reflection artifact reduction achieved at the same location of the finger using synthetic aperture PAFUSion. Figure 9(a) shows the PAFUSion image. It is clear that all the artifacts that are identified by using plane-wave PAFUSion (Fig. 8(a)) are identified in this case too. The only difference between the two approaches is the changed relative amplitudes of the identified artifacts (possibly caused by the motion of finger in between measurements). Figure 9(b) shows the PA image corrected using synthetic aperture PAFUSion in which reflection artifacts are significantly reduced. Reflection artifact reduction ratio values for all the marked features in the PA image are summarized in dB scale in Table 2 to quantitatively validate and compare the efficiency of synthetic aperture PAFUSion with plane-wave PAFUSion in reducing reflection artifacts.

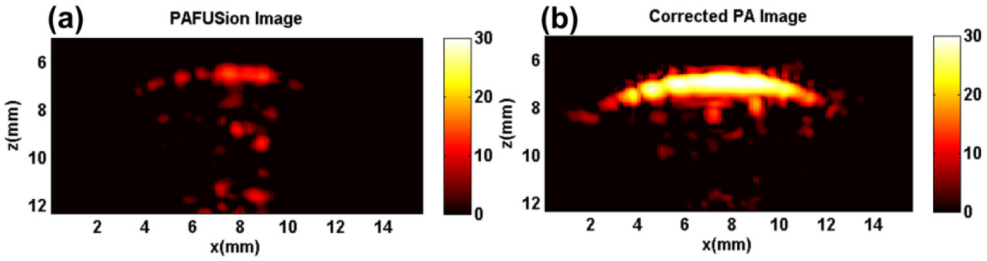

Fig. 9. Synthetic aperture PAFUSion to identify and reduce reflection artifacts in the *in vivo* measurement: (a) PAFUSion image, (b) corrected PA image.

Table 2 demonstrates that the pixel intensities of features a_5 to a_9 are significantly reduced in the corrected PA image using both the approaches, with an average reduction of around 13

Biomedical Optics EXPRESS

dB, substantiating the hypothesis that these are reflection artifacts. The intensities of features a_1 to a_4 are reduced only by around 1 dB which is significantly less than what was measured for a_5 to a_9, substantiating the hypothesis that these are real PA sources. Slight differences are evident in the corrected PA images and consequently the intensity reduction ratio for both approaches (especially for features a_5 to a_9). Most likely, this may have been caused by slight movement of the volunteer's finger during the collection of synthetic aperture US data which is the last acquisition step in the measurement chain.

Table 2. Comparison of Intensity Reduction Ratios (IRR) achieved using plane-wave and synthetic aperture PAFUSion for the *in vivo* measurement

Region of interest	a_1	a_2	a_3	a_4	a_5	a_6	a_7	a_8	a_9
IRR (dB) (Plane-wave)	1.3	1.1	1	1	5	14	16	18	20
IRR (dB) (Synthetic aperture)	1.2	1.2	1	1	3.5	10	16.2	14	14.5

5. Discussion

The phantom and the *in vivo* results demonstrated that both the plane-wave and the synthetic aperture backpropagation-based PAFUSion are capable of identifying and significantly reducing reflection artifacts in epi-mode PA imaging using a commercial US scanner and an integrated US/PA probe. With both the approaches, reflection artifacts were reduced on an average by 13 dB in both the phantom and the *in vivo* studies. We demonstrated identification and strong reduction of reflection artifacts in superficial tissue and near the bone surface of the finger. In a conventional image, these artifacts may well be misinterpreted as small blood vessels, influencing the diagnosis of e.g. inflammation in rheumatoid arthritis, thus demonstrating the importance of PAFUSion in identifying and reducing them.

The goal of this paper was to quantitatively compare the plane-wave and the synthetic aperture approach. As hypothesized in the theory section, our results give a direct confirmation that the plane-wave PAFUSion – while requiring fewer acquisitions – is more suited for reduction of reflection artifacts in clinical epi-PA imaging, when the skin absorption is the main cause of reflection artifacts (skin mimicking layer/skin was the most important artifact source in the phantom and the *in vivo* study). Based on the hypothesis that superposition of a sparse number of plane transients may be sufficient to mimic most part of the PA wavefield of a skin layer, plane-wave PAFUSion was performed with only 33 acquisitions (33 angles) covering +/– 16 degrees, compared to 64 acquisitions (scan through all 64 elements and one element transmitting at a time) used in the synthetic aperture approach. This will benefit a clinical scenario where real-time display is highly desired, by increasing the frame rate by around 2 times when using the plane-wave approach. In addition, a lower number of acquisitions will also help minimize tissue motion during PAFUSion data acquisition and thus improve subtraction accuracy. Apart from spatial misalignment between the PA image and the PAFUSion image, tissue motion in-between successive pulse-echo acquisitions can lead to phase cancellation in the superposition of the backpropagated S^*. A smaller number of acquisitions that are required for PAFUSion will therefore benefit subtraction accuracy. If the skin layer is less curved in the PA image, an even smaller angle range and thus a smaller number of plane-waves will be sufficient to mimic the inward propagating wavefield from the skin. In an extreme case, if the skin is a straight-line feature, then plane-wave PAFUSion can be done with a single US plane-wave transmitted at the angle perpendicular to that feature. However, to determine the minimum number of angles required to mimic inward propagating wavefield of the skin melanin layer in an average situation requires further investigation.

Biomedical Optics EXPRESS

The efficiency of reducing reflection artifacts (intensity reduction ratio) that were caused by both the extended features and point-like absorbers in the phantom experiment were found to be similar for both approaches. In any clinical applications of epi-mode PA imaging, skin is considered to be the most important artifact source because of the high light fluence on the skin surface. Under this circumstance, plane-wave PAFUSion will be an appropriate choice because it is more favorable in terms of acquisition speed required for freehand clinical applications. On the other hand, if the main reflection artifact source is a point-like absorber as in interstitial PA imaging (high PA signal from/near the optical fiber/needle tip causing reflection artifacts) [20–22], synthetic aperture PAFUSion will be the better choice, because the full range of the angular aperture of the probe is required to mimic as much as possible of the inward propagating wavefield from a point-like PA source. If the point source is located near the probe, only a sub-aperture of all probe transducer elements – the ones that are located within the probe's angular aperture – can effectively contribute to backpropagation towards the point source. In this case, the number of elements required for the element-by-element approach may even be smaller than the number of required angles for the plane wave approach. However, prior knowledge about the position of the PA source (can be obtained with the guidance of PA and US data) is essential to select the required set of elements for doing synthetic aperture PAFUSion in this situation.

The similar performance of the plane-wave and the synthetic aperture approach was expected, because the two approaches are – mathematically seen –equivalent. Plane-wave transmissions can be regarded as superposition of single-element transmissions, and vice-versa. A slight difference may result from plane wave edge effects, i.e. the divergent waves that emanate from the aperture edges owing to the limited probe aperture. Similar edge waves are expected for the synthetic aperture approach when backpropagating – over the limited aperture – the signal from a plane PA transient. However, a residual difference between the two approaches may result from the specific implementation of the directional filtering functions (Eq. (1)) that can yield a small level of cross-talk between different filtering directions owing to the limited probe aperture. This effect, if present, was not noticeable in our study.

Both, the plane-wave and the synthetic aperture backpropagation approach, are based on the assumption that ultrasound attenuation of the backpropagated PA transients from the probe to the PA source is negligible. Frequency-dependent attenuation will, however, influence the temporal profile of the mimicked echoes in a depth-dependent way. Frequency-dependent attenuation and dispersion can therefore add to a spatially dependent amplitude and phase mismatch between real and mimicked reflection artifacts. Whereas the effect of attenuation was not noticeable so far in the in-vivo study, it may become significant when imaging inside strongly attenuating tissue. A correction for expected average bulk attenuation may be possible, but not for spatial variations that are a priori unknown. In addition to attenuation, spatial variations of speed-of-sound (SoS) can influence the result. Moderate spatial variations may not have a strong influence, as long as the phase distortion of the outward-travelling PA wavefront can be accurately inverted by backpropagation. Strongly heterogeneous tissue (spatial variations of SoS and acoustic impedance), however, can lead to scattering and inward-reflections of the outward travelling PA wavefront that cannot be mimicked by backpropagation, introducing amplitude and waveform distortions. A single-sided representation for backpropagation of PA signals, based on the multidimensional Marchenko equation proposed by Van der Neut *et al.* (to be published) will be potentially capable of reducing these reflections that occur at superficial tissue structures both below and above strong PA sources.

Both in the phantom and *in vivo* measurements (plane-wave and synthetic aperture PAFUSion), the relative amplitudes and phases of the actual and the identified reflection artifacts were found to be spatially dependent. Consequently, a correction with one-step amplitude and phase matching for all features was not possible. A reason for relative

Biomedical Optics EXPRESS

amplitude and phase differences could be that - because the distance to the skin/phantom surface is small (5-10 mm) - the to-be-simulated PA sources are not in the elevation focal distance of the probe (24 mm) which results in a distance-dependence of the pressure amplitudes. In this situation, scaling of pressure amplitudes based on the distance from the geometrical focus of the probe may be required to avoid the problem of relative amplitude difference when using PAFUSion. A single amplitude and phase matching step was used for the *in vivo* study (for example: Fig. 8b shows corrected PA image obtained with one amplitude and phase matching step). In this case, artifacts are strongly reduced, while the intensity of real PA features remains basically unchanged. Therefore, we hypothesize that it will be possible to adaptively choose a spatially dependent matching function for amplitude and phase by optimizing local image contrast. In cases where the artifact waveforms in the PA image and the PAFUSion image differ significantly, subtraction may not yield satisfactory results even after phase matching. Differences in waveform are possible in spite of the waveform matching, e.g. when the limited aperture of the probe does not allow to accurately mimic the PA wavefront, or when strongly acoustically scattering or attenuating structures distort the wavefront in a way that cannot be compensated for by backpropagation. In such cases, it may be beneficial to remove phase sensitivity by image subtraction after envelope detection. This approach was successfully demonstrated for removing reflection artifacts in the context of interstitial PA imaging of brachytherapy seeds [12]. In a situation where artifacts interfere with real PA signal, however, envelope subtraction – being a non-linear operation – can result in a corrected PA amplitude that not only depends on the real PA signal amplitude but also on the relative amplitude and phase of artifact and PA signal.

In a clinical situation, the PAFUSion image itself will already be relevant for identifying true features in the PA image. However, reduction of reflection artifacts in the PA image has the added benefit of identifying true PA features that are else hidden by reflection artifacts. The approach of matching the amplitude/phase of each reflection artifact separately and correcting the artifacts one by one real-time during the measurement is a feasible option. For example, clinicians can be given an option to click on features in the PAFUSion image (identified artifacts) and automatic correction of that particular feature by suitable scaling of pixel intensities and phases can be potentially implemented. Alternatively, the image can be split into sub-regions in each of which an automatic correction is performed.

In the present study, we demonstrated reduction of sparsely distributed and distinct reflection artifacts. Similar to speckle in ultrasound images, PA images can also contain diffuse speckle caused by interference of randomly distributed echoes. Speckle artifacts become significant in comparison to real PA signal when imaging deep (> 1 cm) inside tissue [23, 24], but not at the imaging depth of the presented in-vivo results. Even though PAFUSion is in principle able to accurately mimic PA echo speckle, the presented results did not have sufficient dynamic range to demonstrate it.

The implementation of plane-wave and synthetic aperture PAFUSion is straightforward in any system with sufficient transmission and acquisition control. Even though PAFUSion processing is done offline in this study, real-time implementation of plane-wave and synthetic aperture PAFUSion is potentially feasible in any US/PA system. The system used for this study can perform interleaved US and PA measurements at a high frame rate (200 Hz limited by maximum permissible light exposure) and we envisage implementing real-time PAFUSion in this system for future clinical studies.

PAFUSion requires the identification of the time interval [0, T] that encompasses the direct signal of superficial absorbers (e.g. skin) but excludes the part of the signal where echoes become significant. A wrong choice of T will result in missing of artifacts when too short, and in backpropagation of echoes resulting in new artifacts when too long. This problem is common to both the synthetic-aperture and the plane-wave PAFUSion approach. In a situation where no a priori information on T exists, this choice can be based in an automatic way on PA image features. Potential ways could be to only include PA signals

Biomedical Optics EXPRESS

above a threshold, only include PA signals until a pre-defined depth below skin, or vary T within a pre-defined range to optimize a certain criterion of corrected image quality (such as e.g. minimize the root-mean-square pixel intensity within a ROI). The alternative clutter reduction approaches that were mentioned in the introduction [14,17] are able to distinguish overlapping direct signals and echoes. Even though – in an ideal case – the role of T for differentiating direct signal and clutter becomes obsolete with these techniques, they are expected to benefit from a similar approach to minimize errors that may occur in practice due to a mismatch between model and experimental reality.

6. Conclusions

In summary, a comparison of plane-wave and synthetic aperture PAFUSion in a commercial US scanner used in combination with an integrated US/PA probe demonstrates strong reduction of in-plane reflection artifacts (average reduction of 13 dB) in phantom and *in vivo* measurements using both approaches. Our results demonstrate that plane-wave PAFUSion requiring fewer acquisitions holds more potential than the synthetic aperture approach for reduction of reflection artifacts in clinical epi-PA imaging, in situations where the skin is the main reflection artifact source.

Funding

The research leading to these results has received funding from the European Community's Seventh Framework Programme (FP7/2007-2013) under grant agreement n° 318067, the European H2020 program (CVENT project, Contract number: 731771), and the Swiss Science Foundation (grant no. 205320-144443).

Acknowledgments

Authors acknowledge Dr. Altaf Hussain for his insightful discussions and help. Lalithai Ramachandran is thanked for volunteering the measurements.

Competing financial interests

The authors declare no competing financial interests.